Emission of singly and doubly charged light fragments from C_{60}^{r+} $(r=4-9)$ in Xe^{25+}-C_{60} collisions

S. Martin, L. Chen, R. Brédy, J. Bernard, M. C. Buchet-Poulizac, A. Allouche, and J. Désesquelles
Laboratoire de Spectrométrie Ionique et Moléculaire, Université Lyon 1, UMR CNRS No. 5579, 43 Boulevard du 11 Novembre 1918, 69622 Villeurbanne Cedex, France
(Received 1 April 2002; published 26 December 2002)

Asymmetrical fission of C_{60}^{r+} $(r=4-9)$ ions are studied in Xe^{25+}-C_{60} collisions at 100 keV impact energy ($v \approx 0.18$ a.u.). The branching ratios for the emission of a singly or a doubly charged light fragment, C_m^+ or C_m^{2+}, are measured for each initial charge state *r*. The measured *m*-dependent branching ratios for the singly charged C_m^+ fragment emission channels are reproduced using a simple statistical model. The ionization energies $I(C_{60-2n}^{q+})$ for even numbered fullerenes C_{60-2n}^{q+} $(q=1-5, 8;\ n=1-4)$ and $I(C_{2n}^+)$ for singly charged light fragments C_{2n}^+ $(n=1-4)$ are estimated by the density-functional theory. The total branching ratio for the C_m^{2+} emission channels is found to increase from less than 2 to 25% when the charge *r* of the parent ion C_{60}^{r+} increases from 5 to 9.

DOI: 10.1103/PhysRevA.66.063201 PACS number(s): 36.40.Qv, 36.40.Wa, 61.48.+c

I. INTRODUCTION

Fragmentation of highly charged clusters exhibits a rich complexity of dissociation channels and a large variety of dynamical processes [1–4]. C_{60} fullerene is a highly stable system with strong bonds and constitutes an interesting case to study the fragmentation of clusters with large charge state [5–7]. Many experiments aimed at the observation of the coupling between the electronic excitation and vibronic degrees of freedom have been devoted to C_{60} molecules using laser excitation [8]. For ultrashort pulse duration ($\sim$ femtoseconds), the ionization mechanism is a direct multiphoton ionization process, whereas for longer pulse duration (picoseconds), the coupling to the vibration occurs during the laser excitation time, and the fragmentation processes are observed. In collisions between highly charged ions (HCI) and C_{60} at low velocities ($v \approx 0, 1$ a.u.), the interaction time is very short (a few femtoseconds). Highly charged stable C_{60}^{r+} with *r* up to 10 can be produced by electron transfer from the C_{60} to the HCI at large impact parameters without excitation of the C_{60} molecules [9,10]. These processes are, to some extent, comparable to the ultrashort laser pulse excitations. However, for collisions at small impact parameters, the C_{60} molecules are not only ionized but also heated.

The excitation mechanism in these short-distance collisions is still a matter of discussion. In collisions with singly charged projectiles at impact parameters smaller than the size of C_{60}, nuclear and electronic stopping power produces hot C_{60} molecules undergoing asymmetrical fragmentation and multifragmentation [11]. In collisions with highly charged projectiles, only a small part of hot C_{60} molecules is related to rontal collisions. It is therefore necessary to propose another excitation mechanism for hot C_{60}^{r+} issued from outside C_{60} cage collisions. For impact parameters slightly larger than the size of the C_{60}, a large number of electrons are transferred simultaneously to the projectile at small interaction distances, leading to a sudden screening of the projectile nuclear charge. Fast energy rearrangement between the captured electrons occurs during the interaction time, and several electrons can occupy highly excited Rydberg states. These loosely bound electrons can be recaptured by the charged C_{60} in highly excited states, leading to a strong electronic excitation of the C_{60} molecule. A similar target excitation process via electron recapture in the preceding part of the collision has been already suggested in HCI-atom collisions to explain the Rydberg transition lines of the target [12].

In collision experiments, the excitation energy of the target C_{60}^{r+} depends notably on the initial charge, core size, and collision velocity of the projectile as shown in several experiments devoted to excitation studies [13–15]. For a given C_{60}^{r+} charge state, lower excitation energy is obtained using projectiles with higher charge states and at higher velocities. In the $Xe^{30+}+C_{60}$ collisions at 300 keV ($v=0.3$ a.u.), the fragmentation ratio, i.e., the number of unstable C_{60}^{r+} divided by the summation of the numbers of stable and unstable C_{60}^{r+}, has been measured to be about 5% [7] for C_{60}^{4+} ions. Larger fragmentation ratio for the same ions C_{60}^{4+} has been measured to be about 50% in collisions with a projectile at lower charge state $Ar^{8+}+C_{60}$ at 56 keV ($v=0.24$ a.u.).

Other important factors that determine the fragmentation pattern are the charge state and the size of the cluster. In our previous experiments using $Ar^{8+}+C_{60}$ collisions, detailed information concerning the asymmetrical fission of C_{60}^{3+}, C_{60}^{4+}, and C_{60}^{5+} has been obtained by correlation measurements of the charged fragments. For C_{60}^{3+} parent ions, the evaporation of C_2 is dominant while for C_{60}^{5+}, the asymmetrical fission is the major process. For C_{60}^{4+}, a competition between the evaporation and fission channels is observed [13] and the emissions of C_2^+, C_4^+, C_6^+, and C_8^+ have been measured in coincidence with C_{58}^{3+}, C_{56}^{3+}, C_{54}^{3+}, and C_{52}^{3+} fullerene ions, respectively [16]. These singly charged light fragments are attributed to the loss of C_n^+ chains from the C_{60}^{r+} cage via the so-called ''unzipping'' mechanism. The odd-numbered light fragments, such as C^+, C_3^+, C_5^+, have been observed in coincidence with C_{58}^{3+}, C_{56}^{3+}, and C_{54}^{3+} ions, respectively, showing that a

neutral carbon atom was also emitted. For the parent ions C_{60}^{5+} [17], events with three charged fragments C^+, C_3^+, and C_{56}^{3+} have been observed. The velocity correlation analysis of C^+ and C_3^+ shows that the two light fragments are emitted sequentially with an extremely short lifetime in the intermediate odd-numbered fullerene states C_{59}^{4+} or C_{57}^{4+}. This observation gives a tentative explanation why the odd-numbered fullerenes have been rarely observed in the TOF spectrum in fragmentation experiments. The emission of a doubly charged light fragment from a C_{60}^{5+} parent ion in the channels $C_{60}^{5+} \rightarrow C_{60-m}^{3+} + C_m^{2+}$ has been also observed in Ar^{8+}-C_{60} collisions [18]. The population distribution of these channels has been measured as a function of the number m of carbon atoms of the light fragment C_m^{2+} ($m=6-12$). A maximum has been found around $m=8$ showing a shift towards higher mass compared to the m distribution of singly charged light fragments C_m^+ in channels $C_{60}^{5+} \rightarrow C_{60-m}^{4+} + C_m^+$, for which the maximum is around $m=2$. This observation is in good agreement with a simple fission barrier analysis [4,18].

Using projectiles at higher charge states, highly charged C_{60}^{r+} ions can be prepared. In Xe^{30+}-C_{60} collisions, the fragmentation ratio and the branching ratios between C_2 evaporation, asymmetrical fission, and multifragmentation processes have been measured as a function of the charge of C_{60}^{r+}, with r up to 9 [7]. In the present work, we report on the m-dependent relative branching ratios of C_m^+ and C_m^{2+} light-fragment emission from asymmetrical fission of C_{60}^{r+} ($r=4-9$) in Xe^{25+}-C_{60} collisions. The experimental data are compared with theoretical distributions obtained using a statistical model. To estimate the fission barrier for each reaction channel, the ionization energies $I(C_{60-2n}^{q+})$ for the ionization reaction $C_{60-2n}^{(q-1)+} \rightarrow C_{60-2n}^{q+} + e^-$ ($q=1-8$; $n=1-4$) and $I(C_{2n}^+)$ for $C_{2n} \rightarrow C_{2n}^+ + e^-$ ($n=1-4$) have been calculated using the density-functional theory (DFT) for the most stable isomers of the fullerenes and the C_{2n} chains, respectively.

II. EXPERIMENT

The experimental setup [7] is presented in Fig. 1. Xe^{25+} projectile ions delivered by the ECR at AIM in Grenoble are accelerated to 100 keV and intercepted perpendicularly by a beam of C_{60} molecules. The outgoing projectiles Xe^{23+}, on which two captured electrons are stabilized ($s=2$), are selected by an electrostatic analyzer in order to get a maximum initial population on C_{60}^{r+} ($r=3-9$) parent ions (see Ref. [7], Fig. 4). Ejected electrons and charged C_{60} or fragments are extracted from the interaction region by a transverse electric field of 1 kV/cm. Electrons are accelerated towards a semiconductor detector (PIPS Canberra) polarized at 25 kV. The electron collection efficiency is optimized using an intermediate focusing electrode, and is estimated here to be 89%. The signal of the detector PIPS amplified and sent to an analog-digital converter (AD 811 Ortec) for pulse-height analysis therefore provides the information on the number n of emitted electrons in the collision.

On the other side of the extraction region, recoil ions are accelerated over a distance of 1 cm by an electric field of 2 kV/cm, and sent through a time-of-flight (TOF) tube ($\ell = 32$ cm) to a detector composed of two multichannel plates (MCP). In order to increase the detection efficiency, the ions are postaccelerated towards the first MCP polarized at about -5 kV. Behind the second MCP (5 mm), multianodes of 61 pixels (4.8 mm^2 per pixel) are linked to 61 individual discriminators (2735 DC Lecroy). The 61 signals are sent to two multihit 32-channel time digital converters (TDC) (3377 Lecroy). Under these experimental conditions, the detection efficiency of recoil ions is estimated to be 75% for singly charged fragments C_m^+ ($m=1-11$). Discriminator levels for signals from multianodes are set to get a balance between a good detection efficiency and a low probability for a singly charged light fragment to activate more than one neighboring anode. The relative probabilities for an ion C_m^+ ($m=1-11$) to activate one, two, and three anodes are measured to be 0.72, 0.22, and 0.06. On the contrary, for highly charged fullerene ions C_{60-2n}^{r+} ($r>4$), the probability to activate three anodes is found maximum. This information is useful to differentiate two ions with the same mass over charge ratio for which the lines on a TOF spectrum are mixed, as for example, the stable C_{60}^{6+} and the singly charged fragment C_{10}^+ issued from multifragmentation process.

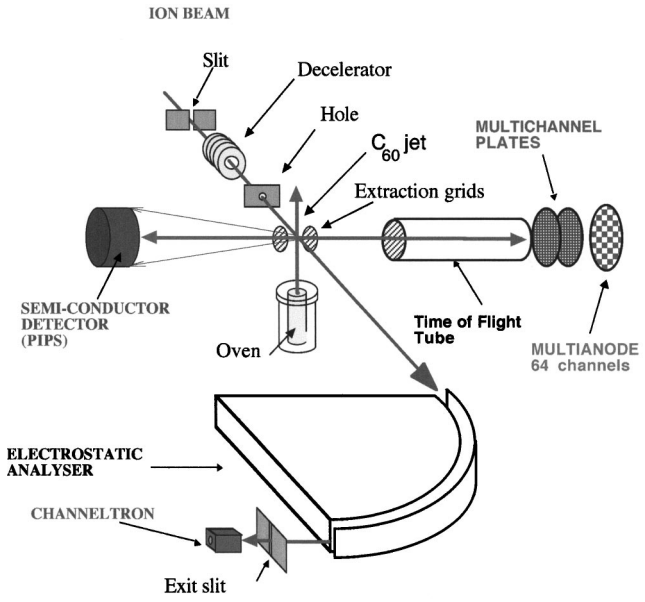

FIG. 1. Experimental setup.

Multicoincidence measurements are performed in event-by-event mode and all data are recorded in list mode. The delayed Xe^{23+} ($s=2$) outgoing projectile ion signal is used as trigger for the AD converter of the electron signal, and provides a common stop signal to the two units of TDC. The amplitude of the electron signal, the hit times on each pixel of the multianodes, and the pixel channels (spatial positions) activated in each event are recorded. From the electron number conservation law, the charge of the target C_{60}^{r+} after the collision can be estimated by $r=n+s$ (in fact, $r=n+2$ with $s=2$). Measurements under identical conditions were performed during 20 h with a flux of about 300 events per sec.

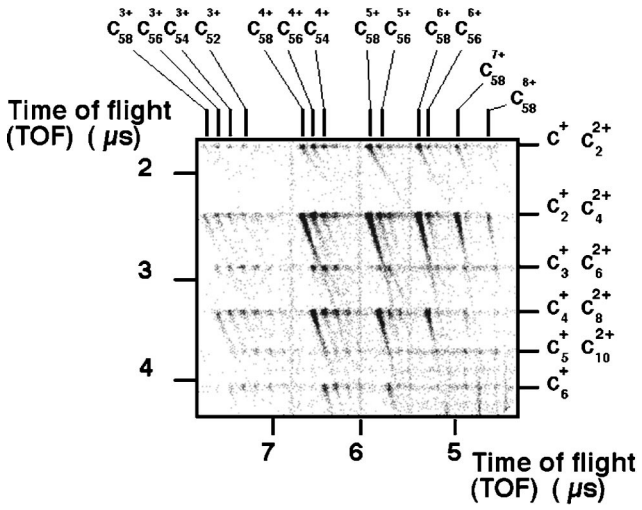

FIG. 2. Correlated two-fragment recoil ion (RI-RI) spectrum. Horizontal axis: the TOF of the heavy fragment; vertical axis: the TOF of the correlated light fragment. The activated pixel number associated with the heavy fragment is selected to be higher or equal to 3 to ensure the detection of a multiply charged fullerence.

III. DATA ANALYSIS

Figure 2 shows a two-dimensional (2D) spectrum of recoil ions (RI, RI) corresponding to events with two charged fragments. One of them is a multiply charged fullerene and the other one is a light fragment. The TOF (t_1) of the last detected fragment (the heavier one) is plotted along the horizontal axis, and the TOF (t_2) of the correlated light fragment along the vertical axis. Note that the TOF scales are reversed due to the common STOP data-acquisition mode of the TDC. The number n of detected electrons is selected in the range from 1 to 8, so that the charge r of the parent ions C_{60}^{r+} is ranged from 3 to 10. The detection of a multiply charged fullerene ion in an asymmetrical fission process is assured by the selection of events for which at least three neighboring pixels were activated by the heavy fragment. The main spots (C_{60-m}^{q+}-C_m^+, $q=3-8$, $m=2, 4, 6, 8$) are characterized by the total number of carbon atoms on the two fragments, equal to 60. They are unambiguously attributed to the fission channels $C_{60}^{r+} \rightarrow C_{60-m}^{q+} + C_m^+$ ($r=q+1=4-9$; $m=2, 4, 6, 8$), and the associated populations are given in the Table I. The long oblique tails that prolong the spots towards shorter flight time of C_{60-m}^{q+} and longer flight time of C_m^+ are due to the delayed fission of C_{60}^{r+} ions all along the path between the extraction grids. Other spots (C_{60-m}^{q+}-$C_{m'}^+$; $m>m'$) with a total number of carbon atoms smaller than 60 are also observed in Fig. 2. Each of them cannot be associated to a fission channel unambiguously. For instance, two fission channels can be attributed to the spot (C_{58}^{4+}-C^+), $C_{60}^{6+} \rightarrow C_{58}^{4+} + C_2^{2+}$, and $C_{60}^{6+} \rightarrow C_{58}^{4+} + C^+ + C^+$ (when only one of the two C^+ fragments is detected in the last case). The possible contribution of another channel with a parent quintuply charged ion C_{60}^{5+}, $C_{60}^{5+} \rightarrow C_{58}^{4+} + C^+ + C$ is excluded by analyzing the tail of the spot (C_{58}^{4+}-C^+). It is notable that the slope of this spot is very different from that of the spot (C_{58}^{4+}-C_2^+), which is attributed to the fission of C_{60}^{5+} without doubt. In a delayed fission process, the slope of the tail depends sensitively on the charge difference between the parent ion and the fullerene fragment. A larger angle with respect to the vertical axis as shown by the spot (C^{4+}-C^+) compared to the spot (C_{58}^{4+}-C_2^+) is the typical signature of a fullerene ion C_{58}^{4+} carried at the beginning of the extraction field by a parent ion with two more charge units C_{60}^{6+}. The decay of C_{60}^{6+} to C_{58}^{4+} is possible by the loss of a doubly charged fragment C_2^{2+} or by the quasisimultaneous emission of two C^+ fragments [17]. This analysis is available for all other spots (C_{58}^{q+}, C^+) with $q>4$.

TABLE I. Event number counts of the spots ($C_{60-m}^{(r-1)+}$-C_m^+), ($C_{60-m}^{(r-2)+}$-C_m^{2+}), and ($C_{60-m}^{(r-2)+}$-C_m^+-C_m^+) measured in two-fragment or three-fragment (RI-RI) correlated spectra and the relative branching ratios R_b for the associated asymmetrical fission channels. The charge r of the parent ions C_{60}^{r+} ranges from $r=4$ to 9.

Fission channels	C_{60}^{4+}		C_{60}^{5+}		C_{60}^{6+}		C_{60}^{7+}		C_{60}^{8+}		C_{60}^{9+}	
	Counts	R_b	Counts	R_b	Counts	R_b	Counts	R_b	Counts	R_b	Counts	R_b
$C_{58}^{r-1}+C_2^+$	1243	0.335	7582	0.501	8212	0.527	4118	0.582	922	0.572	208	0.451
$C_{56}^{r-1}+C_4^+$	1659	0.447	3983	0.263	3197	0.205	929	0.131	62	0.038		0.000
$C_{54}^{r-1}+C_6^+$	307	0.082	809	0.053	444	0.028						0.000
$C_{52}^{r-1}+C_8^+$	156	0.042	188	0.012								0.000
$C_{58}^{r-2}+C_2^{2+}$			18	0.001	363	0.023	325	0.046	122	0.076	90	0.195
$C_{56}^{r-2}+C_4^{2+}$			78	0.005	255	0.016	229	0.032	160	0.099	32	0.070
$C_{54}^{r-2}+C_6^{2+}$			53	0.003	342	0.022	182	0.026				
$C_{52}^{r-2}+C_8^{2+}$			63	0.004	354	0.023	119	0.017				
$C_{58}^{r-1}+C^+ + C^0$	60	0.016	275	0.020								
$C_{56}^{r-1}+C_3^+ + C^0$	224	0.060	214	0.015								
$C_{54}^{r-1}+C_5^+ + C^0$	59	0.015	86	0.006								
$C_{58}^{r-2}+C^+C^+$			175	0.012	1071	0.069	715	0.101	206	0.133	130	0.284
$C_{56}^{r-2}+C_3^+ + C^+$			456	0.030	1347	0.086	392	0.056	131	0.085		
$C_{54}^{r-2}+C_3^+ + C_3^+$							66	0.009				

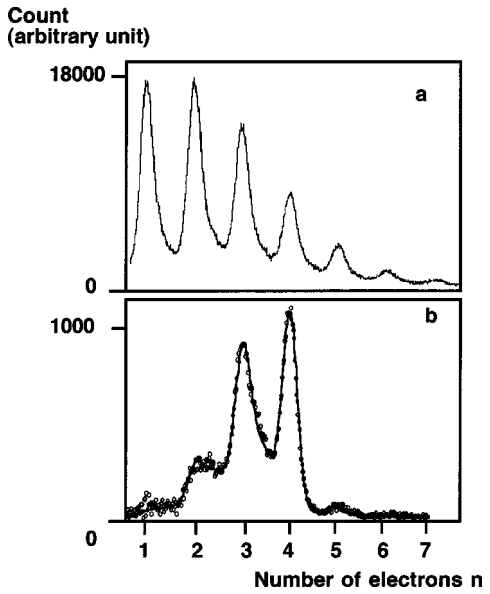

FIG. 3. (a) Electron number spectrum recorded in coincidence with Xe^{23+} outgoing projectiles. (b) Electron number spectrum for events with $n=4$ ejected electrons, recorded in coincidence with Xe^{23+} ($s=2$) and stable C_{60}^{6+} recoil ions. ○, experimental data; continuous line, fit. The $n=1$, 2, 3 peaks are due to the backscattered electron effect and the electron collection efficiency less than 100%. The fit allows us to estimate the electron collection efficiency to be about 89%.

In order to differentiate fragmentation channels issued from different parent ions C_{60}^{r+}, a straight way is to determine the initial charge $r+$ by analyzing the number of ejected electrons. In Fig. 3(a), we present the electron number spectrum for all events, and in Fig. 3(b) we present the $n=4$ electron number spectrum. Events involving four ejected electrons are characterized by the detection of a stable C_{60}^{6+} ion. With $r=6$, $s=2$, one obtains $n=r-s=4$. In Fig. 3(b), the one-, two-, and three-electron peaks are interpreted by the well-known backscattered electron effect of the electron detector PIPS and by a limited electron collection detection efficiency [19]. To reproduce precisely the measured four-electron spectrum, we have adjusted the electron collection detection efficiency and the backscattering probability to be 89% and 16%, respectively. Therefore, a peak in Fig. 3(a), for example $n=3$, is not only attributed to events where three electrons are ejected; it is also partially attributed to events where four, five, or more electrons are actually ejected. Two-fragment spectra of (RI, RI) similar to Fig. 2 are recorded for each selected electron number peak of Fig. 3(a). The obtained (RI, RI) spectrum for a given peak n is then contributed by the asymmetrical fission of the parent ions C_{60}^{r+} with mainly $r=n+2$ and partially $r>n+2$.

A typical two-fragment (RI, RI) spectrum for a selected electron number peak, $n=6$ ($r=8$), is shown in Fig. 4. Three spots, (C_{58}^{7+}-C_2^+), (C_{58}^{6+}-C^+), and (C_{56}^{6+}-C_2^+), are attributed to the C_{60}^{8+} parent ions. The spot (C_{58}^{7+}-C_2^+) corresponds to the main fission channel $C_{60}^{8+}\rightarrow C_{58}^{7+}+C_2^+$. The spots ($C_{58}^{6+}$-$C^+$) or ($C_{56}^{6+}$-$C_2^+$) are attributed principally to the emission of a doubly charged fragment C_2^{2+} or C_4^{2+}, and partially to the

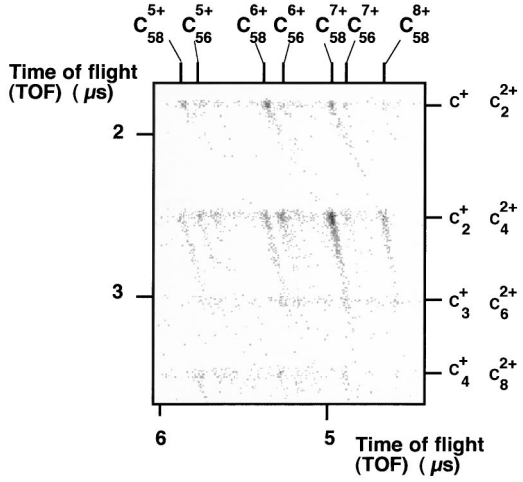

FIG. 4. Correlated two-fragment (RI-RI) spectrum associated with the $n=6$ peak of the electron number spectrum, Fig. 3(a). The main spots (C_{58}^{7+}-C_2^+), (C_{58}^{6+}-C^+), and (C_{56}^{6+}-C_2^+) are attributed to the parents C_{60}^{8+}. Contributions of parent ions at the higher charge state C_{60}^{9+} are also observed.

channels with the emission of two C^+ fragments or two C_2^+ fragments when only one of them is detected. The quasiabsence of the spot (C_{56}^{7+}-C_2^+) shows that the channel $C_{60}^{8+}\rightarrow C_{56}^{7+}+C_2^+ + C_2$ can be neglected. It is in good agreement with the previous finding that the emission of a neutral fragment is negligible for fullerenes with a charge higher than 4 [13]. The spots (C_{58}^{8+}-C_2^+) and (C_{58}^{7+}-C^+) are attributed to channels of the C_{60}^{9+} parent ions, $C_{60}^{9+}\rightarrow C_{58}^{8+}+C_2^+$, $C_{60}^{9+}\rightarrow C_{58}^{7+}+C_2^{2+}$, and $C_{60}^{9+}\rightarrow C_{58}^{7+}+C^+ + C^+$ (when only one C^+ fragment is detected). Other weak spots like (C_{58}^{6+}, C_2^+) and ($C_{58}^{5+}+C_2^+$) are contributed by the parent ions C_{60}^{r+} at lower charge state $r=7$ and 6. It is due to the one or two additional random electrons issued from double collision process. To get pure (RI-RI) spectra associated to each well-defined parent ion C_{60}^{r+}, the analysis began from the (RI-RI) spectrum of the highest charge state C_{60}^{9+} ($n=7$) which is practically pure (the fission of C_{60}^{10+} is not observed). The pure (RI-RI) spectrum of the parent ion C_{60}^{8+} is obtained by the (RI-RI) spectrum of the peak $n=6$ subtracting the contribution of the spectrum of C_{60}^{9+}. The pure (RI-RI) spectrum of the parent ion C_{60}^{7+} is obtained by the (RI-RI) spectrum of the peak $n=5$ subtracting the contribution of the spectrum of C_{60}^{9+} and then that of the corrected spectrum of C_{60}^{8+}, etc.

The populations of three-fragment channels with the quasisimultaneous emissions of two odd-numbered fragments such as $C_{60}^{r+}\rightarrow C_{58}^{(r-2)+}+C^+ + C^+$, $C_{60}^{r+}\rightarrow C_{56}^{(r-2)+}+C^+ + C_3^+$, and $C_{60}^{r+}\rightarrow C_{54}^{(r-2)+}+C_3^+ + C_3^+$; and the successive emission of two even numbered fragments, such as $C_{60}^{r+}\rightarrow C_{56}^{(r-2)+}+C_2^+ + C_2^+$, are obtained from another type of 2D (RI, RI) spectrum showing the correlation between the two light fragments. An example is presented in Fig. 5, which shows a spectrum recorded by selecting events associated to a given electron number peak $n=5$, and characterized by the detection of a fullerene fragment C_{56}^{5+}. The TOF of the two light fragments are plotted in the 2D spec-

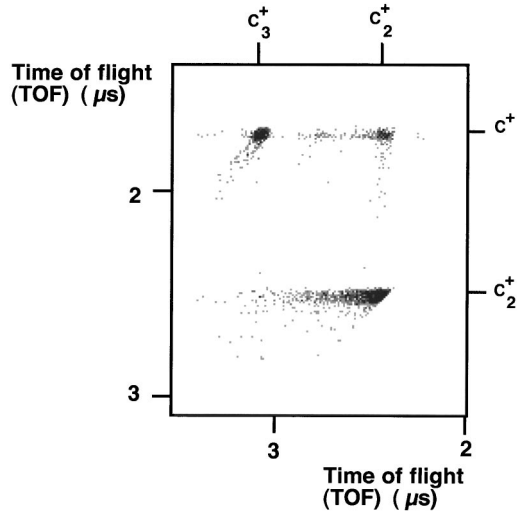

FIG. 5. Correlated three-fragment (RI-RI) spectrum between the two light fragments in coincidence with the selected heavy C_{56}^{5+} ions and the ejected electron number $n=5$. The main spots (C^+-C_3^+) and (C_2^+-C_2^+) are attributed to the reactions $C_{60}^{7+} \rightarrow C_{56}^{5+} + C^6 + C_3^+$ and $C_{60}^{7+} \rightarrow C_{56}^{5+} + C_2^+ + C_2^+$, respectively.

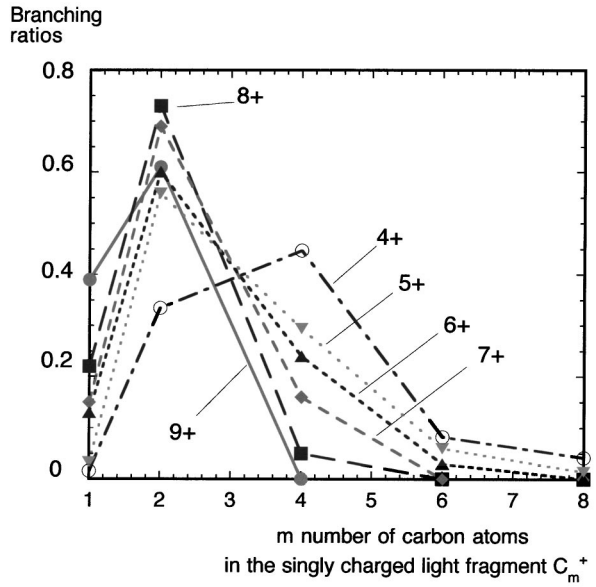

FIG. 6. Relative branching ratios for the asymmetrical fission channels $C_{60}^{r+} \rightarrow C_{60-m}^{(r-1)+} + C_m^+$ as a function of the number of carbon atoms m on the light fragment. To guide the eyes, the data for each parent charge state C_{60}^{r+}, $4 \leqslant r \leqslant 9$, are connected with a line and the associated charge $r+$ is indicated.

trum. The TOF of the heavier one is plotted along the horizontal axis and that of the lighter one along the vertical axis. From the spots (C_1^+, C_3^+) and (C_2^+, C_2^+), we measured the populations of the corresponding channels $C_{60}^{7+} \rightarrow C_{56}^{5+} + C^+ + C_3^+$ and $C_{60}^{7+} \rightarrow C_{56}^{5+} + C_2^+ + C_2^+$. Similar 2D spectra are recorded for $n=5$, in coincidence with the detection of a C_{58}^{5+} or a C_{54}^{5+}, respectively. The spots (C^+,C^+) and (C_3^+,C_3^+) on the two spectra allowed us to measure the populations of the other two channels, $C_{60}^{7+} \rightarrow C_{58}^{5+} + C^+ + C^+$ or $C_{60}^{7+} \rightarrow C_{54}^{5+} + C_3^+ + C_3^+$. The contribution of these three-fragment channels in the two-fragment (RI, RI) spectrum is corrected using the detection efficiency of the monocharged fragments [18]. This correction allows us to determine the populations of the asymmetrical fission channels involving a doubly charged light fragment, $C_{60}^{r+} \rightarrow C_{60-m}^{(r-2)+} + C_m^{2+}$.

IV. RESULTS AND DISCUSSION

The measured relative branching ratios of different fission channels R_b for parent ions C_{60}^{r+} with r ranging from 4 to 9 are presented in Table I. The dominant asymmetrical fission channels for all studied parent ions C_{60}^{r+} are the singly charged light-fragment emissions. The relative branching ratio as a function of the number m of carbon atoms on the light fragment C_m^+ is presented in Fig. 6 for each charge state of the parent C_{60}^{r+}. Only data for even-numbered fragments and for the C^+ fragment are considered, because the contributions of other odd-numbered fragments are very small. Difficulties arise in the determination of the population for the channels $C_{60}^{r+} \rightarrow C_{59}^{(r-1)+} + C^+$. The emission of a C^+ fragment from a C_{60}^{r+} parent ion is followed by a fast sequential emission of another odd-numbered charged fragment C^+ or C_3^+ leading to a contribution to the measured populations of the channels $C_{60}^{r+} \rightarrow C_{58}^{(r-2)+} + C^+ + C^+$ or $C_{60}^{r+} \rightarrow C_{56}^{r-2} + C^+ + C_3^+$. However, the measured population of the last channel is partially contributed by another fission path, $C_{60}^{r+} \rightarrow C_{57}^{(r-1)+} + C_3^+ \rightarrow C_{56}^{(r-2)+} + C^+ + C_3^+$, where the C_3^+ fragment is lost at the first step. The relative contributions of these two paths can be estimated by analyzing the kinetic energy of the light fragment, which depends on the charge of its fission partner. If C^+ is ejected at the first step, the Coulomb repulsion between $C_{59}^{(r-1)+}$ and C^+ is higher than that between $C_{56}^{(r-2)+}$ and C^+ when it is ejected at the second step. For parent ions C_{60}^{5+}, the contributions of the two paths have been estimated to have equal probabilities [17]. In this study, we assume roughly that the contribution of the path where the C^+ is ejected at the first step increases linearly from 50% to 90% as the charge of the parent ion C_{60}^{r+} varies from 5 to 8. For the C_{60}^{8+} parent ions, the emission of C^+ is dominant over that of C_3^+. A population shift towards lighter fragments C^+ and C_2^+ is noted as the charge of the parent C_{60}^{r+} increases. The same shift is remarkable from Table I for doubly charged light fragments.

In order to reproduce theoretically the relative population distribution as a function of m of the singly charged light fragment C_m^+ for each C_{60}^{r+} ion ($r=4-9$), a statistical model based on the Rice, Ramsperger, and Kassel theory is employed [20,13]. We consider a fullerene ion C_{60}^{r+} with internal energy ϵ which is statistically distributed among all vibrational modes. A fission channel is opened as long as a critical energy higher than the inner part of the associated fission barrier B is accumulated in at least one vibrational mode. The relative branching ratio of such a fission channel is then estimated as proportional to $(1-B/\epsilon)^{3p-7}$, with $p=60$ for C_{60}. The fission barrier B for each reaction channel $C_{60}^{r+} \rightarrow C_{60-m}^{(r-1)+} + C_m^+$ is obtained by summing up the

energy change $\Delta_m{}^r$ of the reaction and the outer part of the barrier $B'_m{}^r$ due to the Coulomb repulsion between the two fission partners. The energy change $\Delta_m{}^r$ is calculated as following:

$$\Delta_m{}^r = E_{\rm at}(C_{60}) - V_{\rm ion}^{(r)\prime}(C_{60}) - [E_{\rm at}(C_{60-m}) - V_{\rm ion}^{r\prime-1}(C_{60-m}) + E_{\rm at}(C_m) - V_{\rm ion}^{(1)}(C_m)], \quad (1)$$

where $E_{\rm at}(C_p)$ stands for the atomization energy of the clusters C_p [5] and $V_{\rm ion}^{(z)}(C_p)$ for the z ionization potential of C_p. The atomization energies $E_{\rm at}(C_p)$ for fullerenes ($50 \leqslant p \leqslant 60$) and for light chains ($2 \leqslant p \leqslant 10$) are calculated using the binding energy per atom of Campbell, Raz, and Lovine [21]. The z ionization potential $V_{\rm ion}^{(z)}(C_p)$ is the sum of the successive ionization energies $I(C_p{}^{q+})$ for the reactions $C_p{}^{(q-1)+} \rightarrow C_p{}^{q+} + e^-$ with q varying from 1 to z. $I(C_p{}^{q+})$ is obtained by calculating the energy-level difference between the final and the initial states of each ionization reaction.

The energy levels of fullerenes $C_{60-2n}{}^{q+}$ are calculated with the DFT [22] using the GAUSSIAN code with $B3LYP$ base. The closed-cage geometry of each fullerene C_{58}, C_{56}, C_{54}, and C_{52} is obtained using a successive Stone-Wales rearrangement following C_2 extrusions as described in Ref. [16]. The ring spirals, describing how the pentagons are distributed on these cages, are given in the following:

58:(1,2,9,11,13,15,17,20,23,25,27,29),

56:(1,2,4,9,12,16,19,22,23,24,26,28),

54:(1,2,4,9,12,14,16,19,23,25,27,28),

52:(1,2,4,9,12,14,16,19,21,23,25,28).

The C—C bond distances of each fullerene have been optimized using a semi-empirical method, i.e., modified neglect of differential overlap. Another isomer of C_{56} obtained from C_{60} by direct extrusion of a C_4 carbon chain has been also studied. The energy level of this second isomer is slightly lower (-0.4 eV) than that of the first isomer for the neutral molecule and is higher for the multicharged molecule $C_{56}{}^{5+}$ (0.7 eV). The ionization energy $I(C_{56}{}^{q+})$ for the ionization reaction $C_{56}{}^{(q-1)+} \rightarrow C_{56}{}^{q+} + e^-$ is then the difference between the energy levels associated to the most stable isomers of $C_{56}{}^{(q-1)+}$ and $C_{56}{}^{q+}$. The obtained $I(C_{56}{}^{q+})$ values are very near to those calculated using only the first isomers within a dispersion range of 0.1 eV. So, in the following, for other fullerenes only isomers achieved by successive C_2 extrusions are considered. The results of calculations are shown in Fig. 7 for $I(C_{60-2n}{}^{q+})$ for $n=1-4$, and $q=1-5$ and $q=8$. As expected, the ionization energy increases with decreasing size of the fullerene. Fits were performed to reproduce the theoretical data using the following equation:

$$I(C_{60-2n}{}^{q+}) = W_\infty + \frac{q}{R_0\left(\frac{60-2n}{60}\right)^{1/2}} \times 27.21(\text{eV}), \quad (2)$$

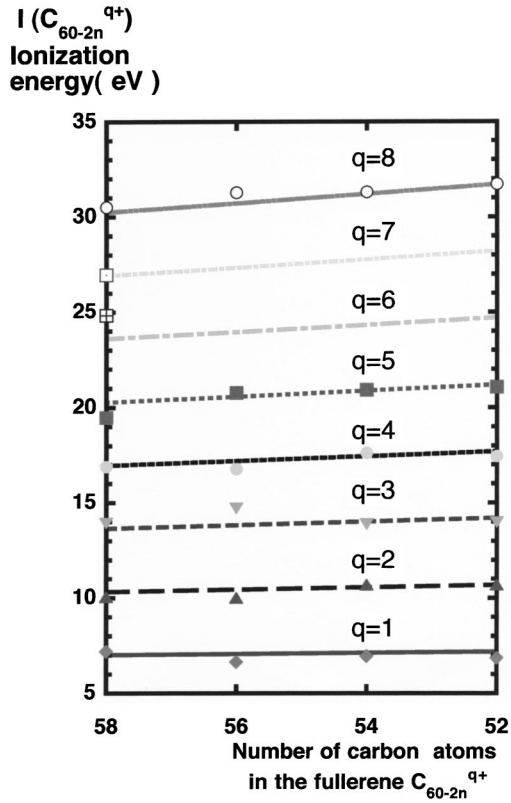

FIG. 7. Ionization energy $I(C_{60-2n}{}^{q+})$ for the reaction $C_{60-2n}{}^{(q-1)+} \rightarrow C_{60-2n}{}^{q+} + e^-$ calculated using the density-functional theory, versus the number of carbon atoms of the fullerene $(60-2n)$ for charge state q varying from 1 to 8. The curves result from the fitted equation (2).

where W_∞ stands for the work function to remove an electron from a neutral fullerene cage and R_0 for the radius of the C_{60} molecule. The term $R_0[(60-2n)/60]^{1/2}$ corresponds to the radius of a fullerene C_{60-2n}, under the assumption that the surface density of the carbon atoms is conserved for all fullerene cages. The best fit is found with $W_\infty = 3.69$ eV and $R_0 = 8.34$ a.u. The ionization energies for odd-numbered fullerenes and for even-numbered fullerenes $I(C_{60-2n}{}^{q+})$ with $n>4$ and for $q=5-7$ are estimated with this relation. The first ionization energies $I(C_{2n}{}^+)$ of even-numbered carbon chains are calculated using the same method with a complete geometry optimization for each molecule. The values, 12.15, 11.25, 10.11, and 9.53 eV for $C_2{}^+$, $C_4{}^+$, $C_6{}^+$, and $C_8{}^+$, respectively, are in good agreement with the data of the Ref. [23]. For the odd-numbered carbon chains, we use the first ionization energies given in the same reference [23], 11.26, 11.4, 10.7, 10, and 9.4 eV for C^+, $C_3{}^+$, $C_5{}^+$, $C_7{}^+$, and $C_9{}^+$, respectively.

The energy change $\Delta_m{}^r$ has been calculated for the reactions $C_{60}{}^{r+} \rightarrow C_{60-m}{}^{(r-1)+} + C_m{}^+$ with m ranging from 1 to 8 and for r from 4 to 9. The outer part of the Coulomb barrier $B'_m{}^r$, depending on the charge of the two fission partners and the fission distance R, is estimated as $B'_m{}^r = (r-1)/R$. Under the multistep assumption for the fission process [24], R is considered as the critical distance for single-electron transfer from the initially evaporated neutral fragment C_m to

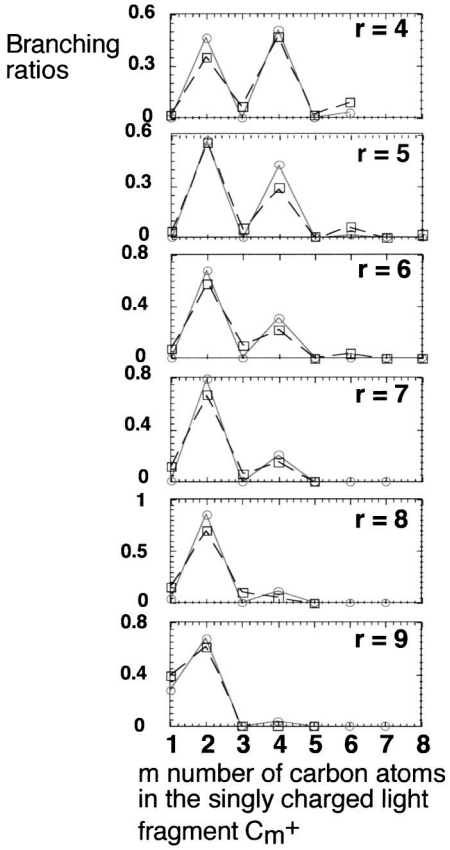

FIG. 8. □ connected by broken lines, experimental *m*-dependent branching ratios for the fission channels $C_{60}^{r+} \rightarrow C_{60-m}^{(r-1)+} + C_m^+$ with r ranging from 4 to 9. ○ connected by continuous lines, branching ratios calculated with the statistical model.

the residual fullerene C_{60-m}^{r+}. It increases linearly from 17 to 18.5 a.u. as the number of carbon atoms of the light fragment increases from 2 to 8. These values are extrapolated from measurements of the kinetic-energy release in the fission processes $C_{60}^{5+} \rightarrow C_{60-m}^{4+} + C_m^+$, $m=2$, 4, and 6 [24,25]. The inner part of the fission barrier B for the emission of a C_2^+ fragment is found to be 11.2, 9.8, 8.4, 7.1, 5.8, and 4.5 eV for C_{60}^{r+} with r ranging from 4 to 9. A critical charge state, corresponding to the vanishing of the fission barrier, can be extrapolated for the reaction $C_{60}^{r+} \rightarrow C_{58}^{(r-1)+} + C_2^+$ at $r=12$.

A detailed comparison between the theoretical branching ratios obtained with the statistical model and the experimental population distributions for the fission channels $C_{60}^{r+} \rightarrow C_{60-m}^{(r-1)+} + C_m^+$ is presented in Fig. 8, as a function of the number m of the light fragment for each C_{60}^{r+} parent ion $(4 \leqslant r \leqslant 9)$. In the calculation for $r=4-9$ values, the excitation energy was taken to $\varepsilon = 80$ eV according to Ref. [7], where this value has been adjusted in order to fit the measured fragmentation ratio of C_{60}^{r+} parents ions in Xe^{30+}-C_{60} collisions. On the contrary to the relative branching ratios, the fragmentation ratios are more sensitive to the excitation energy. The global agreement between the calculation and the experiment shows that the statistical model gives a satisfactory description for the asymmetrical fission of multiply charged C_{60}, with the charge of parent ion up to 9 and the mass of the light fragment from 1 to 8. For higher charge states $r>5$, the multifragmentation channels are opened. These channels, probably due to C_{60}^{r+} parent ions with an initial energy much higher than 80 eV, are not considered in the simulation.

Based on the statistical model, for a given parent ion C_{60}^{r+}, the maximum of the branching ratio is associated to the fission channel with the lowest fission barrier. The population shift (Fig. 6) towards lighter fragments C^+ and C_2^+ with increasing charge of the C_{60}^{r+} can be then understood qualitatively in terms of the fission barrier variation as a function of the number m. The energy change Δ_m^r of the fission reaction $C_{60}^{r+} \rightarrow C_{60-m}^{(r-1)+} + C_m^+$ can be considered as the summation of two terms, a positive term contributed by the atomization energy change and a negative term, called Coulomb term Λ, which is associated with the ionization potential change. The positive term decreases with decreasing m value of the light fragment, which favors the very asymmetrical mass division process. In the negative term Λ, the ionization potential of the light fragment $V_{\rm ion}^{(1)}(C_m)$ decreases with increasing m and that of the fullerene heavy fragment $V_{\rm ion}^{(r-1)}(C_{60-m})$ increases with m. For fission reactions with a parent ion C_{60}^{r+} at low charge state $(r<4)$, the variation of the negative term as a function of m is dominated by $V_{\rm ion}^{(1)}(C_m)$, because the variation of $V_{\rm ion}^{(r-1)}(C_{60-m})$ with m is negligible compared to that of $V_{\rm ion}^{(1)}(C_m)$ (Fig. 7). The negative term Λ favors then the fission channels with a heavier fragment C_m^+. When the charge of the parent ion C_{60}^{r+} increases, the variation of $V_{\rm ion}^{(r-1)}(C_{60-m})$ as a function of m plays a more and more important role in the term Λ and becomes dominant for $r>5$. So, for C_{60}^{r+} at high charge state, both the negative and the positive terms favor the asymmetrical mass division channels, leading to the measured branching ratio R_b shifted towards lighter fragments C^+ and C_2^+.

The emission of a doubly charged light fragment from a C_{60}^{r+} parent ion is a relatively weak channel. However, it becomes more important with increasing charge r. The total branching ratios for the emission of singly charged light fragments (C_m^+) and that of doubly charged light fragments (C_m^{2+}) are presented in Fig. 9 as a function of the charge r. They are obtained from Table I by the summations $\Sigma_m R_b(C_m^+)$ and $\Sigma_m R_b(C_m^{2+})$, respectively, for each parent ion C_{60}^{r+}. The total branching ratio for the emission of doubly charged light fragments $\Sigma_m R_b(C_m^{2+})$ increases from less than 2% to 25% with the increasing charge of the parent ion r from 5 to 9. This tendency can be interpreted by analyzing the fission barrier variation of these two types of channels versus the charge of C_{60}. The fission barrier for the emission of a C_2^+ fragment, for example, is found to decrease with increasing charge r. This variation is mainly due to the negative Coulomb term $[\Lambda = -V_{\rm ion}^{(r)}(C_{60}) + V_{\rm ion}^{(r-1)} \times (C_{58}) + V_{\rm ion}^{(1)}(C_2)]$ in the energy change calculation of the reaction $C_{60}^{r+} \rightarrow C_{58}^{(r-1)+} + C_2^+$. If the difference between $V_{\rm ion}^{(r-1)}(C_{60})$ and $V_{\rm ion}^{(r-1)}(C_{58})$ is neglected, this term is approximated as $\Lambda \approx -\Gamma(C_{60}) + V_{\rm ion}^{(1)}(C_2)$, which decreases ac-

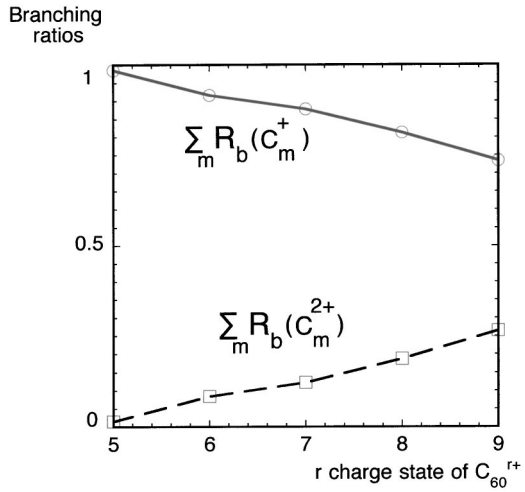

FIG. 9. ○: total branching ratio $\Sigma_m R_b(C_m{}^+)$ of the singly charged light-fragment emission channels versus the charge state r of the parent ions $C_{60}{}^{r+}$. □: total branching ratio $\Sigma_m R_b(C_m{}^{2+})$ of the doubly charged light-fragment emission channels versus r.

tually with increasing charge r. In a similar way, for the fission channel $C_{60}{}^{r+} \rightarrow C_{58}{}^{(r-2)+} + C_2{}^{2+}$, the Coulomb term is approximated as $\Lambda' \approx -I^r(C_{60}) - I^{r-1}(C_{60}) + V_{\rm ion}^{(2)}(C_2)$, which decreases more rapidly with increasing charge r. At low charge state $C_{60}{}^{5+}$, the very different branching ratios of the two types of fission channels suggest that the barrier for the $C_m{}^{2+}$ emission channel is much higher than that of the $C_m{}^+$ emission channel. As the charge r becomes higher, the barrier for the emission of a doubly charged fragment $C_m{}^{2+}$ decreases faster than that for the $C_m{}^+$ emission channel. At high charge state $C_{60}{}^{9+}$, the barriers for the two types of fission channels are so close that the relative branching ratios become comparable.

V. CONCLUSION

By multicoincidence analyses of the projectile final charge state, the ejected electron number, the TOF, and the activated pixel numbers of the charged fragments, we have measured the light-fragment mass-dependent branching ratios of the asymmetrical fission of $C_{60}{}^{r+}$ parent ions with the charge r ranging from 4 to 9. The measured m-dependent population distributions for the singly charged fragment emission channels $C_{60}{}^{r+} \rightarrow C_{60-m}{}^{(r-1)+} + C_m{}^+$ are relatively well reproduced with a simple statistical model showing that the asymmetrical fission of $C_{60}{}^{r+}$ with a charge state r up to 9 can be described by similar thermally activated evaporative process. To estimate the fission barriers, the ionization potentials of multiply charged fullerenes and light singly charged C_m chains are calculated with the density-functional theory. A population shift towards lighter fragments C^+ and $C_2{}^+$ is observed with the increasing charge of the $C_{60}{}^{r+}$. It is interpreted qualitatively in terms of the fission barrier variation as a function of the number m. The doubly charged light-fragment emission channels $C_{60}{}^{r+} \rightarrow C_{60-m}{}^{(r-2)+} + C_m{}^{2+}$ are also observed. The total branching ratio of these channels increases from less than 2% to 25% with the charge of the parent ion varying from 5 to 9. This tendency is due to the fact that the fission barrier of the $C_m{}^{2+}$ emission channel decreases faster than that of the $C_m{}^+$ emission channel as the charge of the $C_{60}{}^{r+}$ parent ion increases. The multifragmentation channels become important for $C_{60}{}^{r+}$ parent ions with $r > 6$. Studies taking account of both asymmetrical fission and multifragmentation of $C_{60}{}^{r+}$ will be performed in the near future.

ACKNOWLEDGMENT

This work was supported by the Région Rhône-Alpes under Grant Nos. 97027-223 and 97027-283, of the Convention Recherche, Program Emergence.

[1] U. Näher, S. Bjørnholm, S. Frauendorf, F. Garcias, and C. Guet, Phys. Rep. **285**, 245 (1997).
[2] O. Echt and T. D. Märk, in *Clusters of Atoms and Molecules*, edited by H. Haberland, Springer Verlag Series in Chemical Physics Vol. 56 (Springer, Berlin, 1994), Vol. 2, p. 183.
[3] C. Bréchignac, P. H. Cahuzac, F. Carlier, and M. de Frutos, NIM B **88**, 91 (1994); C. Brechignac *et al.*, in *Large Clusters of Atoms and Molecules*, *NATO Advanced Studies Institute, Series E*, edited by T. P. Martin (Kluwer Academic, Dordrecht, 1996).
[4] U. Näher, S. Frank, N. Malinowski, U. Zimmermann, and T. P. Martin, Z. Phys. D: At., Mol. Clusters **31**, 191 (1994).
[5] E. E. B. Campbell, in *Clusters of Atoms and Molecules*, edited by H. Haberland, Springer Verlag Series in Chemical Physics Vol. 52 (Springer, Berlin, 1994), Vol. 2, p. 331.
[6] S. G. Kim and D. Tomanek, Phys. Rev. Lett. **72**, 2418 (1994).
[7] S. Martin, L. Chen, A. Denis, R. Brédy, J. Bernard, and J. Désesquelles, Phys. Rev. A **62**, 022707 (2000).
[8] E. E. B. Campbell, K. Hansen, K. Hoffmann, G. Korn, M. Tchaplyguine, M. Wittmann, and I. V. Hertel, Phys. Rev. Lett. **84**, 2128 (2000).
[9] B. Walch, C. L. Cocke, R. Völpel, and E. Salzborn, Phys. Rev. Lett. **72**, 1439 (1994).
[10] J. Jin, H. Khemliche, M. H. Prior, and Z. Xie, Phys. Rev. A **53**, 615 (1996).
[11] T. Schlathölter, O. Hadjar, R. Hoekstra, and R. Morgenstern, Phys. Rev. Lett. **82**, 73 (1999).
[12] M.N. Gaboriaud, M. Barat, P. Roncin, and V. Sidis, J. Phys. B **27**, 4595 (1994).
[13] S. Martin, L. Chen, A. Denis, and J. Désesquelles, Phys. Rev. A **57**, 4518 (1998); L. Chen *et al.*, *ibid.* **59**, 2827 (1999).
[14] O. Hadjar, P. Földi, R. Hoekstra, R. Morgenstern, and T. Schlathölter, Phys. Rev. Lett. **84**, 4076 (2000).
[15] H. Cederquist, A. Fardi, K. Haghighat, A. Langereis, H. T. Schmidt, S. H. Schwartz, J. C. Levin, A. Sellin, H. Lebius, B. Huber, M. O. Larsson, and P. Hvelplund, Phys. Rev. A **61**, 022712 (2000).
[16] P. W. Fowler and D. E. Manolopoulos, *An Atlas of Fullerenes* (Oxford University Press, Oxford, 1995).
[17] L. Chen, S. Martin, R. Brédy, J. Bernard, and J. Désesquelles, Phys. Rev. A **64**, 031201 (2001).

[18] L. Chen, S. Martin, R. Brédy, J. Bernard, and J. Désesquelles, Europhys. Lett. **58**, 375 (2002).
[19] F. Aumayr, G. Lakits, and H. Winter, Appl. Surf. Sci. **47**, 139 (1991).
[20] K. S. Kassel, J. Phys. Chem. **32**, 225 (1928).
[21] E. E. B. Campbell, T. Raz, and R. D. Levine, Chem. Phys. Lett. **253**, 261 (1996).
[22] A. D. Becke, J. Chem. Phys. **98**, 5648 (1993); M. J. Frisch, G. W. Trucks, H. B. Schlegel, G. E. Scuseria, M. A. Robb, J. R. Cheeseman, V. G. Zakrzewski, J. A. Montgomery, Jr., R. E. Stratmann, J. C. Burant, S. Dapprich, J. M. Millam, A. D. Daniels, K. N. Kudin, M. C. Strain, O. Farkas, J. Tomasi, V. Barone, M. Cossi, R. Cammi, B. Mennucci, C. Pomelli, C. Adamo, S. Clifford, J. Ochterski, G. A. Petersson, P. Y. Ayala, Q. Cui, K. Morokuma, D. K. Malick, A. D. Rabuck, K. Raghavachari, J. B. Foresman, J. Cioslowski, J. V. Ortiz, A. G. Baboul, B. B. Stefanov, G. Liu, A. Liashenko, P. Piskorz, I. Komaromi, R. Gomperts, R. L. Martin, D. J. Fox, T. Keith, M. A. Al-Laham, C. Y. Peng, A. Nanayakkara, C. Gonzalez, M. Challacombe, P. M. W. Gill, B. Johnson, W. Chen, M. W. Wong, J. L. Andres, C. Gonzalez, M. Head-Gordon, E. S. Replogle, and J. A. Pople, GAUSSIAN (Gaussian, Inc., Pittsburgh, PA, 1998).
[23] K. Raghavachari and J. S. Binkley, J. Chem. Phys. **87**, 2191 (1987).
[24] P. Scheier, B. Dünser, and T. D. Märk, Phys. Rev. Lett. **74**, 3368 (1995).
[25] L. Chen, J. Bernard, R. Brédy, J. Désesquelles, and S. Martin, Phys. Scr. **116**, 1 (2001).